Power Engineering and Engineering Thermophysics
https://www.acadlore.com/journals/PEET

Thermodynamic Performance of Advanced Adiabatic Compressed Air Energy Storage in Deep Wells Considering Unsteady Wellbore–Rock Heat Transfer

Dongjin Xu[1,2], Zhiwen Xu[1,2*], Shuqi Niu[1,2], Feipeng He[1,2], Yukai Guo[3], Yong Wang[4], Xiangyang Luo[5], Wenping Liu[6]

[1] School of Petroleum Engineering, Yangtze University, 430100 Wuhan, China
[2] State Key Laboratory of Low Carbon Catalysis and Carbon Dioxide Utilization, Yangtze University, 430100 Wuhan, China
[3] Quality Safety Environmental Protection Technology Supervision Center, PetroChina Changqing Oilfield Company, 710018 Xi'an, China
[4] Oil and Gas Technology Research Institute, PetroChina Changqing Oilfield Company, 710018 Xi'an, China
[5] Ground Emergency Repair Center, Zhongyuan Oilfield Company, SINOPEC, 457001 Puyang, China
[6] Oil Production Engineering Research Institute, PetroChina Daqing Oilfield Co., Ltd., 163453 Daqing, China

* Correspondence: Zhiwen Xu (2024720462@yangtzeu.edu.cn)

Received: 04-26-2025 **Revised:** 06-16-2025 **Accepted:** 06-29-2025

Citation: D. J. Xu, Z. W. Xu, S. Q. Niu, F. P. He, Y. K. Guo, Y. Wang, X. Y. Luo, and W. P. Liu, "Thermodynamic performance of advanced adiabatic compressed air energy storage in deep wells considering unsteady wellbore–rock heat transfer," *Power Eng. Eng. Thermophys.*, vol. 4, no. 2, pp. 131–148, 2025. https://doi.org/10.56578/peet040205.

Abstract: Repurposing deep abandoned oil and gas wells for advanced adiabatic compressed air energy storage (AA-CAES) has attracted increasing attention; however, reliable performance assessment is challenged by the complex thermal behaviour induced by the large aspect ratio of deep wells and the long-term interaction between the gas column and surrounding formations. In particular, simplified heat transfer assumptions commonly adopted in existing models may lead to non-negligible deviations in capacity and efficiency predictions. To address this issue, a coupled thermodynamic framework is established that accounts for gas column gravity effects, geothermal temperature gradients, and unsteady heat conduction in the surrounding rock. Different wellbore heat transfer boundary representations and operational strategies are systematically examined to clarify their influence on the thermal and energetic performance of deep-well AA-CAES systems. The analysis indicates that under low mass flow rate conditions, the extended wellbore length promotes effective heat exchange between the compressed air and the surrounding rock, restricting the average temperature variation along the wellbore and leading to compression and expansion processes that deviate markedly from ideal adiabatic behaviour. When a constant wall temperature boundary is employed to represent long-term formation heat transfer, the predicted storage capacity is reduced by 6.12% compared with conventional adiabatic assumptions. In addition, sliding-pressure operation exhibits superior adaptability to the thermal characteristics of deep wells, increasing the round-trip efficiency (RTE) from 48.82% to 60.99 relative to constant-pressure operation. At low flow rates, extended thermal relaxation further enhances heat dissipation, resulting in a modest increase in effective energy storage density (ESD). These results highlight the role of surrounding rock formations as a distributed thermal buffer and underscore the importance of incorporating realistic heat transfer modelling and appropriate operational strategies in the thermodynamic design of deep-well AA-CAES systems.

Keywords: Deep wells; Advanced adiabatic compressed air energy storage; Wellbore–rock heat transfer; Unsteady-state thermal behaviour; Thermodynamic operation strategy

1 Introduction

With the rapid expansion of new energy installed capacity, building a new power system has become an urgent necessity. However, traditional power systems struggle to address the peak-shaving and safety challenges posed by high penetration of renewable energy due to insufficient flexible regulation resources [1–4]. Advanced adiabatic

compressed air energy storage (AA-CAES) has emerged as a research hotspot due to its large capacity and long lifespan advantages. However, its large-scale deployment is constrained by the stringent geological distribution of salt caverns. In response, repurposing vast numbers of abandoned oil and gas wells as storage caverns not only enables direct reuse of their deep pressurized spaces but also effectively overcomes site selection bottlenecks, offering significant engineering value and economic potential [5–8].

Extensive research has been conducted by scholars worldwide on the thermodynamic performance and integration characteristics of AA-CAES systems. At the system integration level, Yang et al. [9] were the first to reveal the significant influence mechanism of non-linear temperature variation in the air storage chamber on the expansion machine inlet conditions and system efficiency. Han et al. [10] demonstrated that cascaded thermal energy utilization in combined cooling, heating, and power (CCHP) mode can significantly enhance the overall energy efficiency of the system. Pang and Han [11] further quantified the negative degradation effect of variable-efficiency compressors on overall system performance under non-design conditions. Additionally, some researchers have validated the performance enhancement of novel working fluids like supercritical CO_2 and solar-assisted heating on system performance [12, 13].

Unlike conventional salt caverns or surface storage tanks, abandoned oil and gas wells possess unique geometric characteristics—deep burial, narrow diameters, and large vertical spans—resulting in more complex heat transfer mechanisms [14]. Regarding the flow-heat coupling characteristics on the wellbore side, Ezekiel et al. [15] earlier highlighted the significant sensitivity of system thermodynamic performance to unsteady formation heat transfer. Huang et al. [16] further elucidated the strong coupling mechanism between dynamic flow and heat transfer processes within the wellbore, indicating that neglecting this effect leads to substantial deviations in thermal state predictions. Schmidt et al. [17] demonstrated through analytical-numerical comparisons the necessity of precise numerical heat transfer models under complex boundary conditions for capturing transient temperature fluctuations; Ma et al. [18] emphasized that establishing detailed heat exchanger-wellbore coupling models in unsteady flow fields is fundamental to accurately predicting system round-trip efficiency (RTE). Regarding specific heat transfer behaviors: Sarmast et al. [19] explicitly demonstrated that non-adiabatic effects in the wellbore significantly alter gas temperature evolution trajectories; Houssainy et al. [20] demonstrated, through a comparison of adiabatic and isothermal limits, that rock heat transfer intensity critically constrains the gas's thermodynamic trajectory and the amplitude of its fluctuations; Zhang et al. [21] proposed an innovative approach for geothermal-energy storage coupling using abandoned wells; Han et al. [22] found through comparative studies that rock mass heat transfer can mitigate severe fluctuations in gas temperature to some extent. Although these studies have advanced understanding at the mechanism level, existing system-level research predominantly relies on the "adiabatic/isothermal black-box" assumption. This approach fails to account for the unique long-to-diameter ratio geometry of abandoned wells and overlooks the dynamic coupling effects between deep-well transient heat transfer and surface unit operations, making it difficult to guide practical engineering applications.

More critically, the thermodynamic evolution within the wellbore is influenced not only by heat transfer through the surrounding rock but primarily by the active control of the unit's operating strategy. The operating strategy directly determines system efficiency and lifespan, currently falling into two main categories: constant pressure and sliding pressure [23–27]. Regarding the optimization of constant pressure strategies, Han et al. [28] pointed out that while constant pressure operation stabilizes the unit's operating conditions, the throttling process causes significant pressure loss; Cui et al. [29] proposed a near-isothermal system optimization fixed-pressure strategy that improved certain performance metrics, though its adaptability under variable conditions remains limited. Xiao et al. [30] employed a constant-power control strategy combining throttling with air injection, revealing a trade-off between output power stability and system thermal efficiency. Compared to sliding-pressure strategies, the latter has gradually become a research focus due to its throttle-free characteristics. Sarmast et al. [31], based on the coverage-percentage method, pointed out that the significant temperature and pressure fluctuations in the reservoir under sliding-pressure mode limit the system's response coverage to grid supply and demand events, necessitating refined component sizing to balance thermodynamic losses; Zhang et al. [32] demonstrated through day-ahead scheduling comparisons that sliding-pressure design exhibits superior load tracking capability and economic performance in large-scale scenarios when responding to grid fluctuations. Pottie et al. [33] further validated that despite the stable output of isobaric systems, the lower Levelized Cost of Storage and reduced complexity of sliding-pressure (isochoric) designs make them the superior choice for large-scale implementation. However, existing research largely overlooks the nonlinear amplification of throttling effects under deep well high-pressure conditions, and few studies have revealed the optimization mechanism of rock formation "thermal compensation" on slip-pressure performance from a system-level perspective.

Given the limitations of existing models in handling coupled non-steady-state heat transfer in deep wells and variable operating conditions of equipment, this study establishes a lumped-parameter model for abandoned wellbores that integrates the gravitational effects of gas columns, geothermal gradient distribution, and non-steady-state heat conduction in surrounding rock. This model is bidirectionally coupled with a surface-based multi-stage

compression/expansion equipment model. By comparing the effects of adiabatic, constant-temperature, and constant-wall-temperature heat transfer boundary conditions on system thermodynamic behavior, this study quantitatively analyzes the performance differences and throttling losses between sliding pressure and constant pressure strategies. It particularly reveals how sliding pressure operation triggers a thermal compensation mechanism where the surrounding rock transitions from a heat sink to a heat source. This research aims to clarify the coupling laws between wellbore geometric parameters and operational strategies, providing valuable theoretical reference for low-flow-rate, deep-well design of energy storage systems in abandoned oil and gas wells.

2 System Description and Model Assumptions

The AA-CAES system constructed in this study for abandoned oil and gas wells is a thermal system coupling surface energy conversion with underground energy storage. It primarily comprises three-stage compressor units (C1–C3), heat storage systems (HX1–HX6), abandoned wellbore storage chambers, and three-stage expansion units (T1–T3). Based on energy flow direction, system operation is divided into three phases: energy storage, idle, and energy release. Its working principle and process are illustrated in Figure 1.

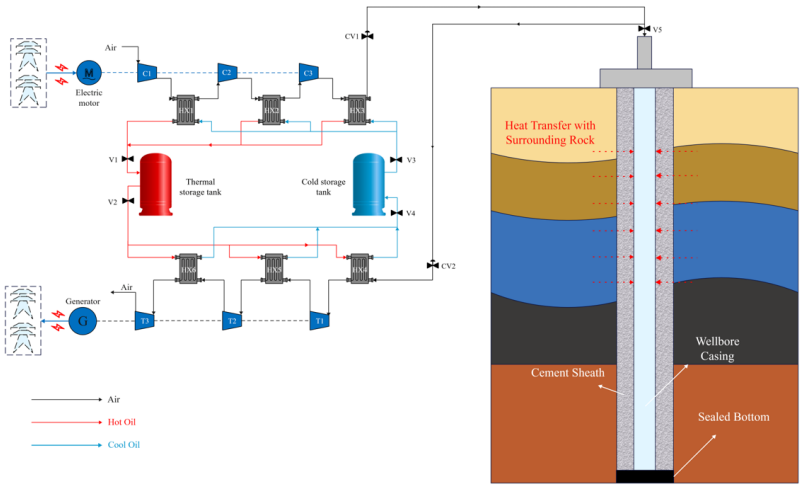

Figure 1. Process flow diagram for advanced adiabatic compressed air energy storage (AA-CAES) system in abandoned oil and gas wells

(1) Energy Storage Phase: Off-peak electricity drives compressors to sequentially compress air. To reduce power consumption and recover thermal energy, inter-stage cooling is employed. High-temperature compressed air releases heat to the thermal storage medium via heat exchangers, then passes through valves into the wellbore after cooling. This converts electrical energy into air pressure potential energy and the thermal storage medium's internal energy.

(2) Static Storage Phase: After energy storage concludes, valves close, transforming the wellbore into a sealed, constant-volume space. Unlike conventional salt caverns, abandoned oil and gas wells feature high aspect ratios and significant geothermal gradients. During static storage, non-steady-state heat transfer occurs between the air and surrounding rock, undergoing thermal relaxation—where gas releases heat to the rock when its temperature exceeds the formation's temperature and absorbs heat when it falls below. This process directly influences the initial state during energy release.

(3) Energy Release Phase: During peak electricity demand, valves open to release high-pressure air from the wellbore. This air is reheated through the thermal storage system before entering an expander to generate electricity, converting stored pressure and thermal energy into electrical energy. The low-pressure exhaust gas is directly vented into the atmosphere after performing work.

To ensure the convergence of the dynamic model solution and highlight key physical processes, the following reasonable assumptions are established based on fundamental laws of engineering thermodynamics [34]: (1) Working fluid properties: Air is treated as an ideal gas; heat transfer oil is treated as an incompressible fluid with constant properties; (2) Heat transfer boundaries: Only unsteady-state heat conduction between the wellbore and surrounding rock is considered (the surrounding rock is treated as a homogeneous semi-infinite medium, with seepage neglected). All surface components are considered adiabatic. Equipment thermal inertia is neglected, and heat exchange processes are treated as quasi-steady-state; (3) Wellbore model: Treated as an airtight, rigid, constant-volume container, neglecting deformation but incorporating pressure correction for column weight; (4) Flow characteristics: Neglecting changes in working fluid kinetic energy and pipeline flow resistance; considering only heat exchanger pressure drop and throttling losses in control valves under constant-pressure mode.

3 Mathematical Modeling

3.1 Compressor and Expander

Considering the operational characteristics of abandoned wells for energy storage, which involve variable backpressure and high pressure ratios, this study employs multi-stage reciprocating piston units to mitigate the risk of turbine machinery surge.

The outlet temperature $T_{\mathrm{c},i}^{\mathrm{out}}$ and power consumption $W_{\mathrm{c},i}$ of the i-th stage compressor are calculated as follows:

$$T_{\mathrm{c},i}^{\mathrm{out}} = T_{\mathrm{c},i}^{\mathrm{in}} \beta_{\mathrm{c},i}^{\frac{n_{\mathrm{c}}-1}{n_{\mathrm{c}}}} \tag{1}$$

$$W_{\mathrm{c},i} = \dot{m}_{\mathrm{c,\,air}}\, C_{\mathrm{p,\,air}}\, \left(T_{\mathrm{c},i}^{\mathrm{out}} - T_{\mathrm{c},i}^{\mathrm{in}}\right) \tag{2}$$

where, the subscripts "c" and "air" denote the compressor and air working fluid, respectively; the subscripts "in" and "out" represent the inlet and outlet states.

Similarly, the outlet temperature $T_{\mathrm{t},i}^{\mathrm{out}}$ and output power $W_{\mathrm{t},i}$ of the i-th stage expander are given by:

$$T_{\mathrm{t},i}^{\mathrm{out}} = T_{\mathrm{t},i}^{\mathrm{in}} \beta_{\mathrm{t},i}^{-\frac{n_{\mathrm{t}}-1}{n_{\mathrm{t}}}} \tag{3}$$

$$W_{\mathrm{t},i} = \dot{m}_{\mathrm{t,air}} c_{\mathrm{p,air}} \left(T_{\mathrm{t},i}^{\mathrm{in}} - T_{\mathrm{t},i}^{\mathrm{out}}\right) \tag{4}$$

where, the subscript "t" denotes the expander; the variable "β" represents the pressure ratio; $\dot{m}$ denotes the mass flow rate; $T_{\mathrm{c},i}^{\mathrm{in}}$ and $T_{\mathrm{t},i}^{\mathrm{in}}$ denote the inlet temperatures of the compressor and expander at stage i, respectively, in K; $\beta_{\mathrm{c},i}$ and $\beta_{\mathrm{t},i}$ denote the compression ratio and expansion ratio at stage i; n_{c} and n_{t} denote the polytropic exponents for compression and expansion, respectively; $\dot{m}_{\mathrm{c,\,air}}$ and $\dot{m}_{\mathrm{t,\,air}}$ represent the air mass flow rates for the compressor and expander, respectively, in kg/s; $C_{\mathrm{p,air}}$ is the specific heat capacity of air at constant pressure, in J/(kg·K).

In actual variable-condition operation, n_{c} and n_{t} are not fixed constants but dynamically adjust with the compression ratio β_i and isentropic efficiency η_{is} at the current stage. According to thermodynamic definitions, the compressor isentropic efficiency $\eta_{\mathrm{c,is}}$, the expander isentropic efficiency $\eta_{\mathrm{t,is}}$, and the polytropic exponent satisfy the following coupling relationship:

$$\eta_{\mathrm{c,is}} = \left(\beta_{\mathrm{c},i}^{\frac{\gamma-1}{\gamma}} - 1\right) / \left(\beta_{\mathrm{c},i}^{\frac{n_{\mathrm{c}}-1}{n_{\mathrm{c}}}} - 1\right) \tag{5}$$

$$\eta_{\mathrm{t,is}} = \left(1 - \beta_{\mathrm{t},i}^{-\frac{n_{\mathrm{t}}-1}{n_{\mathrm{t}}}}\right) / \left(1 - \beta_{\mathrm{t},i}^{-\frac{\gamma-1}{\gamma}}\right) \tag{6}$$

where, γ is the adiabatic index of air (equals 1.4).

The total electrical energy consumed by the system during the energy storage phase, E_{in}, is calculated as follows:

$$E_{\mathrm{in}} = (1/\eta_{\mathrm{motor}}) \int_0^{\tau_{\mathrm{charge}}} \sum_{i=1}^{N_{\mathrm{c}}} W_{\mathrm{c},i}(t)\mathrm{d}t \tag{7}$$

where, the subscripts "charge" denotes the energy storage phase.

Similarly, during the energy release phase, the total electrical energy output E_{out} of the system is calculated as follows:

$$E_{\mathrm{out}} = \eta_{\mathrm{gen}} \int_0^{\tau_{\mathrm{discharge}}} \sum_{i=1}^{N_{\mathrm{t}}} W_{\mathrm{t},i}(t)\mathrm{d}t \tag{8}$$

where, the subscripts "discharge" denotes the energy release phase.

The overall electromechanical efficiencies of the compressor and expander are respectively:

$$\begin{cases} \eta_{\mathrm{motor}} = \eta_{\mathrm{mech,c}} \cdot \eta_{\mathrm{elec,c}} \\ \eta_{\mathrm{gen}} = \eta_{\mathrm{mech,t}} \cdot \eta_{\mathrm{elec,t}} \end{cases} \tag{9}$$

where, the subscripts "motor", "gen", "mech", and "elec" refer to the electric motor, generator, mechanical system, and electrical system, respectively. τ_{charge} and $\tau_{\mathrm{discharge}}$ denote the duration of energy storage and release processes, respectively, in seconds; N_{c} and N_{t} represent the number of compressor and expander stages, respectively; $W_{\mathrm{c},i}(t)$ and $W_{\mathrm{t},i}(t)$ denote the instantaneous power of the i-th stage compressor and expander at time t, in watts; $\eta_{\mathrm{mech,c}}$, $\eta_{\mathrm{mech,t}}$, $\eta_{\mathrm{elec,c}}$, and $\eta_{\mathrm{elec,t}}$ represent the mechanical efficiency of the compressor and expander, and the efficiency of the motor and generator, respectively.

3.2 Heat Exchanger and Thermal Storage

When air flows through a heat exchanger, pressure loss occurs. This can be calculated using the following empirical formula [35]:

$$\Delta p = \frac{0.0083\varepsilon}{1-\varepsilon} \cdot p_{\text{in}} \tag{10}$$

where, p_{in} is the inlet pressure of the heat exchanger, MPa; ε is the heat exchanger efficiency, typically ranging from 0.7 to 0.9.

During the energy storage phase, high-temperature air releases heat to warm the cooling medium. The air outlet temperature $T^{\text{out}}_{\text{air},i,\text{h}}$ at the i-th stage heat exchanger and the cooling medium outlet temperature $T^{\text{out}}_{\text{o},i}$ are calculated as follows:

$$T^{\text{out}}_{\text{air},i,\text{ h}} = (1-\varepsilon)T^{\text{out}}_{\text{c},i} + \varepsilon T^{\text{in}}_{\text{o}} \tag{11}$$

$$T^{\text{out}}_{\text{o},i} = \varepsilon T^{\text{out}}_{\text{c},i} + (1-\varepsilon)T^{\text{in}}_{\text{o}} \tag{12}$$

where, the subscript "o" denotes the thermal oil.

The total heat recovered from the high-temperature storage tank during the energy storage phase is as follows:

$$Q_{\text{hot}} = \sum_{i=1}^{N_{\text{c, h}}} \int_0^{\tau_{\text{charge}}} c_{\text{p,air}} \dot{m}_{\text{c,air}} \left(T^{\text{out}}_{\text{c},i} - T^{\text{out}}_{\text{air},i,\text{ h}}\right) \mathrm{d}t \tag{13}$$

where, the subscript "h" represents the heat exchanger; the subscript "hot" denotes the high-temperature thermal storage tank; $N_{\text{c,h}}$ denotes the number of stages in the compression-side heat exchanger.

Similarly, during the heat release phase, the low-temperature air absorbs heat from the thermal oil. The outlet air temperature $T^{\text{out}}_{\text{air},i,\text{c}}$ at the i-th heat exchanger is:

$$T^{\text{out}}_{\text{air},i,\text{c}} = \varepsilon T^{\text{out}}_{\text{o},i} + (1-\varepsilon)T^{\text{in}}_{\text{air},i} \tag{14}$$

where, $T^{\text{in}}_{\text{air},i}$ denotes the air inlet temperature of the i-th heat exchanger, in K.

3.3 Wellbore Storage Chamber

Based on the laws of conservation of mass and energy, describe the dynamic changes in the average state of air within the wellbore.

(1) Mass Conservation Equation:

$$\frac{\mathrm{d}m_{\text{well}}}{\mathrm{d}t} = \dot{m}_{\text{c,air}} - \dot{m}_{\text{t,air}} \tag{15}$$

where, the subscripts "well" denotes the wellbore.

(2) Energy Conservation Equation:

$$\frac{\mathrm{d}\left(m_{\text{well}} u_{\text{well}}\right)}{\mathrm{d}t} = \dot{m}_{\text{c,air}} h_{\text{in}} - \dot{m}_{\text{t,air}} h_{\text{out}} + \dot{\mathrm{Q}}_{\text{wall}} \tag{16}$$

where, the subscripts "wall" denotes the wellbore wall; m_{well} and u_{well} represent the air mass fraction and specific internal energy within the wellbore, in kg and J/kg, respectively; $\dot{Q}_{\text{wall}}$ denotes the heat exchange rate between the wellbore gas and surrounding rock, in W. Combining the ideal gas equation of state $pV = mR_{\text{g}}T$ with $u = c_{\text{v}}T$, $h = c_{\text{p}}T$, solving Eq. (15) and Eq. (16) simultaneously yields the differential equation system for the average pressure $\bar{p}_{\text{well}}$ and average temperature $\bar{T}_{\text{well}}$ in the wellbore:

$$\begin{cases} \frac{\mathrm{d}\bar{p}_{\text{well}}}{\mathrm{d}t} = \frac{R_{\text{g}}}{c_{\text{v}} V_{\text{well}}} \left[c_{\text{p}} T_{in} \dot{m}_{\text{c, air}} - c_{\text{p}} T_{\text{out}} \dot{m}_{\text{t, air}} + \dot{Q}_{\text{wall}}\right] \\ \frac{\mathrm{d}\bar{T}_{\text{well}}}{\mathrm{d}t} = \frac{R_{\text{g}} \bar{T}_{\text{well}}}{c_{\text{v}} \bar{p}_{\text{well}} V_{\text{well}}} \left[c_{\text{p}} T_{\text{in}} \dot{m}_{\text{c, air}} - c_{\text{p}} T_{\text{out}} \dot{m}_{\text{t, air}} + \dot{Q}_{\text{wall}} - c_{\text{v}} \bar{T}_{\text{well}} \left(\dot{m}_{\text{c, air}} - \dot{m}_{\text{t, air}}\right)\right] \end{cases} \tag{17}$$

where, c_{v} denotes the specific heat capacity at constant volume, J/(kg·K); R_{g} denotes the gas constant for air, J/(kg·K); T_{in} and T_{out} denote the inlet temperature for energy storage and the outlet temperature for energy release, K.

Considering the vertical span of deep wells reaching thousands of meters, the pressure difference caused by the weight of the gas column and the effect of the geothermal gradient on the heat transfer boundary cannot be ignored. Therefore, the following correction equations are introduced:

(1) Gravity Gas Column Pressure Correction

The actual operating pressure of the unit is the wellhead pressure p_{wh}. Within the lumped parameter model framework, the pressure at a depth of $H/2$ is taken as the average wellbore pressure $\bar{p}_{\mathrm{well}}$. Based on the gas hydrostatic equation, the conversion relationship between wellhead pressure and average wellbore pressure is established:

$$p_{\mathrm{wh}}(t) = \bar{p}_{\mathrm{well}}(t) \cdot \exp\left(-\frac{\mathrm{g} \cdot (H/2)}{R_{\mathrm{g}} \bar{T}_{\mathrm{well}}(t)}\right) \tag{18}$$

where, the subscript "wh" denotes the wellhead.

(2) Geothermal Gradient Correction

Simultaneously, the temperature of formation rocks increases linearly with depth z. When calculating surrounding rock heat exchange, the average rock temperature $\bar{T}_{\mathrm{rock}}$ is taken as the constant far-field boundary temperature:

$$\bar{T}_{\mathrm{rock}} = T_{\mathrm{surf}} + G_{\mathrm{geo}} \cdot (H/2) \tag{19}$$

where, the subscripts "rock", "surf", and "geo" denote the surrounding rock, the ground surface, and the geothermal gradient, respectively; g = 9.81 m/s^2; T_{surf} is the surface temperature, taken as 273.15 K; G_{geo} is the geothermal gradient, equals 0.03 K/m; H is the wellbore depth, m.

Based on different definitions of the heat transfer term $\dot{Q}_{\mathrm{wall}}$, this study established three heat transfer models for the gas storage chamber.

(1) Adiabatic model: Assumes no heat exchange, $\dot{Q}_{\mathrm{wall}}$ = 0, suitable for rapid charge-discharge limit analysis.

(2) Isothermal model: Assumes gas temperature remains in thermal equilibrium with the rock, $\bar{T}_{\mathrm{well}}(t) = \bar{T}_{\mathrm{rock}}$.

(3) Constant-wall-temperature model: Closest to real-world conditions, assuming the wellbore wall temperature remains constant at T_{rock}, with gas-wall heat transfer governed by Newton's cooling law [36]:

$$\dot{Q}_{\mathrm{wall}} = h_{\mathrm{w}} A_{\mathrm{well}} \left(T_{\mathrm{rock}} - \bar{T}_{\mathrm{well}}\right) \tag{20}$$

where, h_{w} denotes the combined convective heat transfer coefficient on the inner wall surface of the wellbore, W/(m^2·K); A_{well} represents the effective heat transfer area of the wellbore, m^2. Substituting Eq. (20) into Eq. (17) yields the governing equations for each stage.

3.4 Operating Strategy and Throttling Loss

The abandoned well AA-CAES system is primarily influenced by pressure control strategies. The following analyzes two typical control modes and their models.

(1) Sliding Pressure Operation: Control valves (CV1, CV2) remain fully open, eliminating throttling losses. The unit's operating boundaries dynamically couple with wellhead pressure P_{wh}: the outlet pressure of the third-stage compressor aftercooler and the inlet pressure of the first-stage expander heater maintain equilibrium with P_{wh}. Under this mode, the pressure ratio across stages dynamically adjusts to real-time wellbore conditions.

(2) Constant-pressure operation: Throttling is achieved by varying the opening of control valves to forcibly lock the unit's operating conditions. During energy storage, compressor discharge is throttled to maintain the design upper limit P_{max}; during energy release, wellhead fluid is throttled to maintain the expander inlet pressure at the rated lower limit P_{min}.

While fixed-pressure operation stabilizes conditions, the throttling process incurs significant pressure energy losses. Based on the Gouy–Stodola theorem, the instantaneous energy loss power $\dot{E}x_{\mathrm{loss}}$ is calculated as follows:

$$\dot{E}x_{\mathrm{loss}} = \dot{m} T_0 \Delta s = \dot{m} T_0 R_{\mathrm{g}} \ln\left(\frac{p_{\mathrm{v,\,in}}}{p_{\mathrm{v,\,out}}}\right) \tag{21}$$

where, the subscripts "loss" and "v" refer to the exergy loss and the control valve, respectively; T_0 is the ambient temperature, K; $p_{\mathrm{v,in}}$ and $p_{\mathrm{v,out}}$ are the inlet and outlet pressures of the valve, MPa.

3.5 System Performance Indicators

To quantitatively evaluate the thermodynamic performance of the AA-CAES system in abandoned oil and gas wells, this study selected RTE, energy storage density (ESD), wellbore thermal storage capacity, and throttling thermal loss rate as key evaluation metrics.

(1) System RTE: RTE is the core metric for measuring an energy storage system's energy conversion capability.

$$\eta_{\mathrm{RTE}} = \frac{E_{\mathrm{out}}}{E_{\mathrm{in}}} \tag{22}$$

(2) ESD: ESD is a crucial parameter for evaluating the economic viability of utilizing abandoned wells for energy storage.

$$\rho_{\mathrm{ESD}} = \frac{E_{\mathrm{out}}}{V_{\mathrm{well}}} \tag{23}$$

(3) Wellbore steam storage capacity: Defined as the instantaneous steam stored in the wellbore, Ex_{stored}.

$$Ex_{\mathrm{stored}} = m_{\mathrm{well}} \left[c_{\mathrm{v}} \left(\bar{T}_{\mathrm{well}} - T_0 \right) - T_0 \left(c_{\mathrm{p}} \ln \frac{\bar{T}_{\mathrm{well}}}{T_0} - R_{\mathrm{g}} \ln \frac{\bar{p}_{\mathrm{well}}}{p_0} \right) \right] \tag{24}$$

where, the subscript "stored" denotes the exergy stored in the wellbore; p_0 is the ambient pressure, MPa.

(4) Throttling steam loss rate: Defined as the ratio of total throttling steam loss over the entire cycle, Ex_{total}, to the total steam input to the system, Ex_{in}.

$$\xi_{\mathrm{th}} = \frac{Ex_{\mathrm{total}}}{Ex_{\mathrm{in}}} = \frac{\int_0^{\tau_{\mathrm{cycle}}} \dot{m} T_0 R_{\mathrm{g}} \ln \left(\frac{p_{\mathrm{v,\,in}}(t)}{p_{\mathrm{v,\,out}}(t)} \right) \mathrm{d}t}{E_{\mathrm{in}}} \tag{25}$$

where, the subscripts "th", "total", and "cycle" denote the throttling process, the total amount, and the operation cycle, respectively.

4 Results and Discussions

4.1 Simulation Parameter Design and Validation

To accurately assess the full-cycle dynamic response of AA-CAES systems in abandoned oil and gas wells under complex geological conditions, this study developed a dynamic simulation program based on the .NET platform (a Microsoft software framework). A fourth-order Runge-Kutta algorithm (step size 0.1 s) was employed to solve the system of rigid differential equations, precisely capturing transient characteristics. The simulation targets a decommissioned well with a high geothermal gradient in northwest China. To balance efficiency and accuracy, air properties were linearized, and Therminol-66 heat transfer oil was selected to match high-temperature operating conditions.

Constrained by the narrow borehole diameter and pressure limits of aged casing, a distributed MW-scale system configuration featuring "single-well low-flow rates with modular well clusters" was adopted to mitigate high-velocity friction losses. Single-well injection and production flow rates were set within ranges of 0.05–0.35 kg/s and 0.1–0.7 kg/s, respectively [37], with 0.1 kg/s injection and 0.2 kg/s production selected as the reference operating condition. Key design parameters are listed in Table 1.

Table 1. Main design parameters of the advanced adiabatic compressed air energy storage (AA-CAES) system for abandoned oil and gas wells

Parameter	Value	Unit
Wellbore depth	2500	m
Casing bore (5-1/2 inches)	124.3	mm
Ambient temperature	293.15	K
Ambient pressure	0.101325	MPa
Upper/lower limit pressure for wellbore operation	10 / 4	MPa
Compressor/expander entropy efficiency	0.85	-
Overall efficiency of compressor/expander electromechanical system	0.95	-
Heat exchanger efficiency	0.9	-
Initial temperature of thermal storage medium	293.15	K
Gas injection/production flow rate	0.1 / 0.2	kg/s
Wellbore convective heat transfer coefficient	15	W/m^2·K
Idle time	2	h

To validate the reliability of the constructed model, the "degradation verification method" was employed to compare it with conventional adiabatic gas storage tank experimental data from existing literature [9]. By disabling the rock mass thermal conductivity term in this model, the deep well model was degraded into an adiabatic container model. The verification results are shown in Figure 2. The results demonstrate that the pressure evolution trajectories calculated by this model closely match the experimental data from the literature, with a maximum relative error of only 2.34%. This error primarily stems from deviations between the ideal gas assumption and actual operating conditions, yet remains within the permissible range for system-level energy efficiency assessment. This confirms the model's accuracy in capturing the phase response characteristics during gas charging and discharging, laying a solid foundation for subsequent transient heat transfer analysis in deep wells.

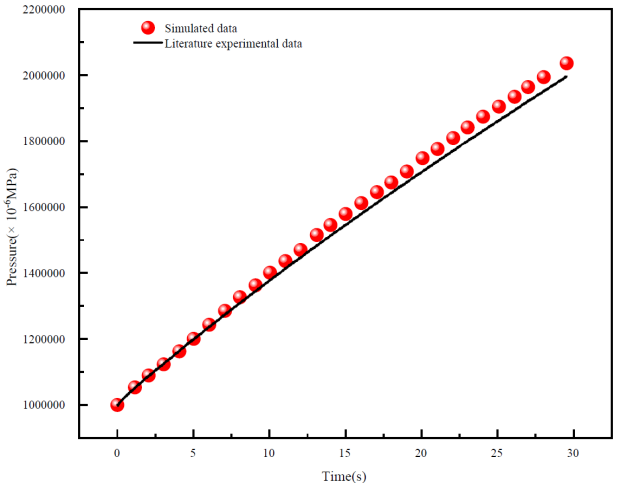

Figure 2. Model validation of dynamic pressure response in the air chamber during inflation

4.2 Impact of Wellbore Heat Transfer Models

Considering the significant non-steady-state heat transfer effects in deep wells, this section compares adiabatic, isothermal, and constant wall temperature models based on a sliding pressure strategy to identify the optimal benchmark heat transfer model for deep well thermal energy storage.

4.2.1 Dynamic evolution of wellbore states

To decouple the effects of operational strategies and specifically examine the thermal dynamic response of the borehole, this study analyzes a typical "energy storage-quiescence-energy release" cycle (Figure 3). During the compression energy storage phase, the adiabatic model exhibits a pronounced "heat accumulation" effect (final temperature reaching 387.95 K) due to its neglect of lateral heat loss, while the constant-temperature model proves overly idealized. In contrast, the constant-wall-temperature model, accounting for both rock cooling and finite convective thermal resistance, calculates a temperature rise of approximately 0.55 K. During the static phase, this model accurately captures the "thermal relaxation" process: the wellbore temperature returns to formation temperature within 2 hours, triggering a natural pressure decay of 0.02 MPa, precisely quantifying the system's self-discharge characteristics.

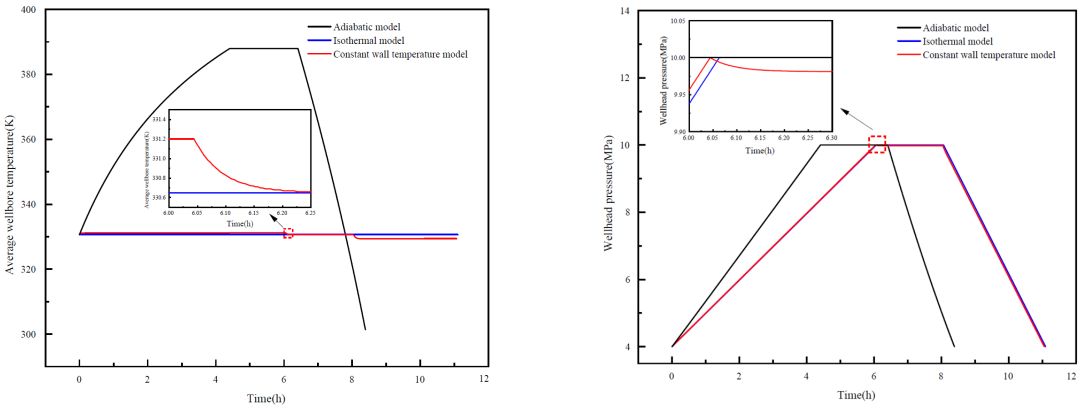

Figure 3. Dynamic evolution of wellbore thermodynamic states under different heat transfer models during charge and discharge processes: (a) Variation of average wellbore temperature; (b) Variation of wellhead pressure

Furthermore, Figure 4 indicates that the self-weight effect of the gas column cannot be ignored. At the end of energy storage, the pressure difference between the well bottom and the wellhead reaches 1.38 MPa. Neglecting gravity correction would significantly underestimate the gas storage capacity. Therefore, coupling the gravity field is a prerequisite for accurately evaluating the performance of deep well AA-CAES.

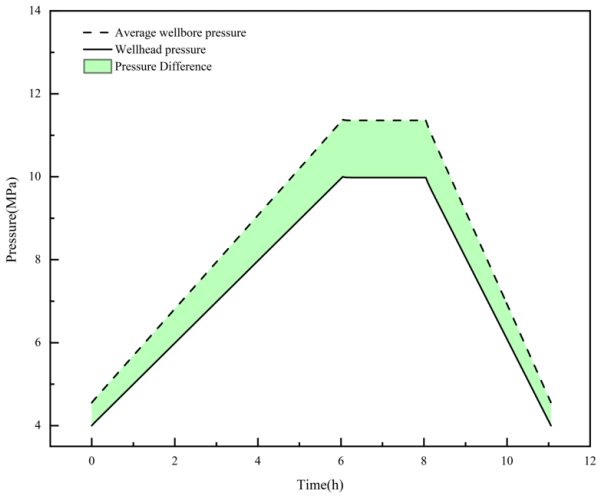

Figure 4. Variations of average wellbore pressure and wellhead pressure under the constant wall temperature model

4.2.2 Radial heat transfer and energy exchange

Based on the constant wall temperature model, Figure 5 reveals the "bidirectional thermal regulation" mechanism of the surrounding rock during the cycle. During the energy storage and quiescent phases, the surrounding rock acts as a "heat sink", suppressing temperature rise and causing isothermal cooling of the working fluid. During the energy release phase, the gas-wall temperature difference reverses, and the surrounding rock transforms into a "heat source". Data indicates that radial heat flux density surges to -19.35 W/m^2 during the late release phase. This pronounced "geothermal compensation effect" effectively mitigates the risk of supercooling during gas discharge.

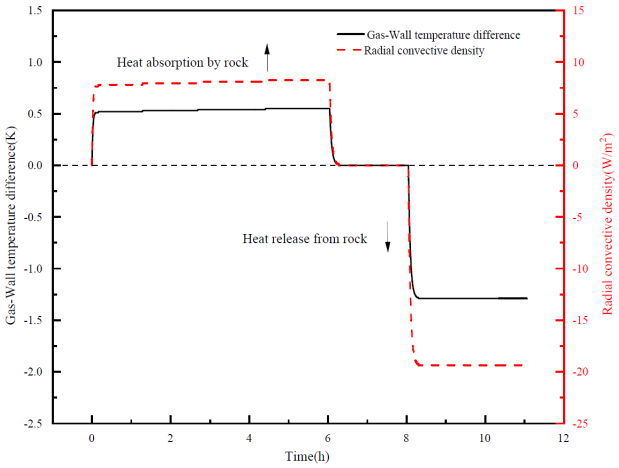

Figure 5. Dynamic evolution of the gas-wall temperature difference and radial heat flux

Integral calculations demonstrate (Figure 6) that while a single cycle dissipates 175.24 MJ of compression heat, it effectively recovers 751.93 MJ of geothermal energy, yielding a net thermal gain of 576.69 MJ. This data confirms that the surrounding rock of abandoned oil and gas wells essentially forms a massive "natural thermal buffer" and "geothermal heat exchanger [38]". It transforms the heat dissipation 'disadvantage' during the idle period into a heat recovery "advantage" during the energy release phase, thereby significantly correcting the prediction deviation of adiabatic models under long-cycle, large-temperature-difference operating conditions.

4.2.3 Impact on system performance evaluation

The accuracy of system performance evaluation relies on precise prediction of working fluid state parameters. Comparing Table 2 with Figure 7 reveals the prediction deviations of the three models. The adiabatic model completely ignores rock heat recovery, causing a sharp drop in wellhead exhaust temperature. It yields a total power generation of only 145.39 kWh and a system efficiency of 54.87%, severely underestimating the actual work potential. The isothermal model assumes an infinitely large heat transfer coefficient, which is overly idealized. Its predicted results (223.32 kWh electricity generation, 61.24% efficiency) exhibit an optimistic bias. The constant-wall-temperature model incorporates both finite heat transfer rates and rock thermal capacity, achieving higher physical

fidelity. Simulations reveal a significant "temperature floor" effect during the energy release phase, where the rock acts as a heat source. The system achieves a RTE of 60.99% and an ESD of 7.31 kWh/m^3. While slightly lower than the constant-temperature model, this result significantly outperforms the adiabatic model. This demonstrates that abandoned wells function as highly efficient "shell-and-tube geothermal heat exchangers". Adopting the constant-wall-temperature model is crucial for correcting the conservative bias of the adiabatic model and establishing an accurate design benchmark.

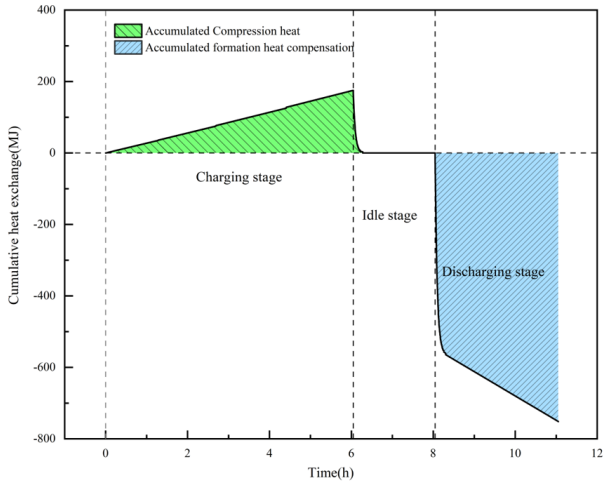

Figure 6. Cumulative heat transfer between the wellbore and surrounding rock

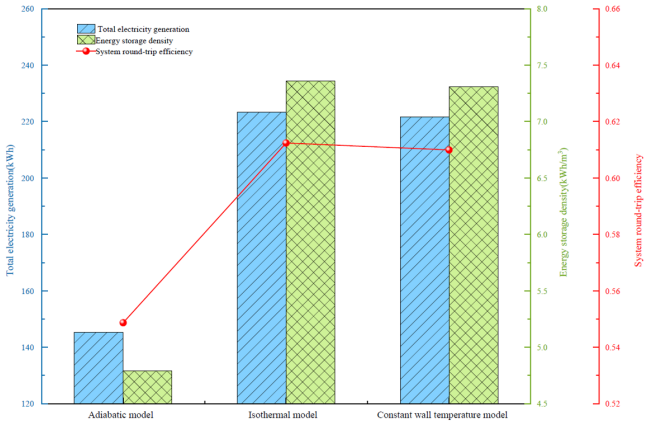

Figure 7. Comparison of the impact of different wellbore heat transfer models on system performance

Table 2. System performance metrics comparison across the entire lifecycle

Performance Metrics	Electricity Consumption (kWh)	Electricity Generation (kWh)	Charge (time/h)	Discharge (time/h)	Effective Air (mass/kg)	System Round-Trip Efficiency (RTE) (%)	Wellbore Exergy Storage (MJ)	Energy Storage Density (ESD) (kWh·m^3)
Adiabatic model	264.98	145.39	4.41	1.98	1425	54.87	1159.34	4.79
Isothermal model	364.66	223.32	6.06	3.03	2182.69	61.24	1413.93	7.36
Constant wall temperature model	363.57	221.76	6.04	3.01	2169.3	60.99	1410.86	7.31

4.3 Performance Comparison of Operation Strategies

Based on the validated constant-wall-temperature model described above, this section focuses on the energy conversion process. It quantitatively compares the thermodynamic characteristics and full-cycle energy efficiency differences between "constant-pressure operation" and "sliding-pressure operation", providing a theoretical basis for optimizing operational strategies under deep-well, high-pressure-differential gas storage conditions.

4.3.1 Thermodynamic process comparison

The core difference in operating strategies lies in the efficiency of utilizing the pressure potential energy of the high-pressure working fluid. Figure 8 reveals the fundamental thermodynamic distinction between the two approaches. Figure 8a shows that the "throttling-first, expansion-later" path in constant-pressure operation leads to substantial dissipation of pressure potential energy. In contrast, sliding-pressure operation eliminates the throttling stage, directly utilizing variable-condition expansion to recover high-grade pressure energy, thereby increasing the actual specific work from 463.03 kJ/kg to 544.91 kJ/kg. Further analysis in Figure 8b indicates that constant-pressure throttling entails significant entropy increase, constituting an irreversible process. In contrast, the sliding-pressure process benefits from constant-wall-temperature heat transfer via deep wellbore rock, causing the expansion path to deviate markedly toward isothermal lines (with variable exponent $n < \gamma$). This confirms that deep formation rock transforms into a real-time heat source during energy release, compensating for expansion-induced temperature drop through "borehole-formation" thermal synergy. This substantially expands the system's work-enthalpy reduction, highlighting the performance enhancement effect of "borehole-formation" thermal synergy.

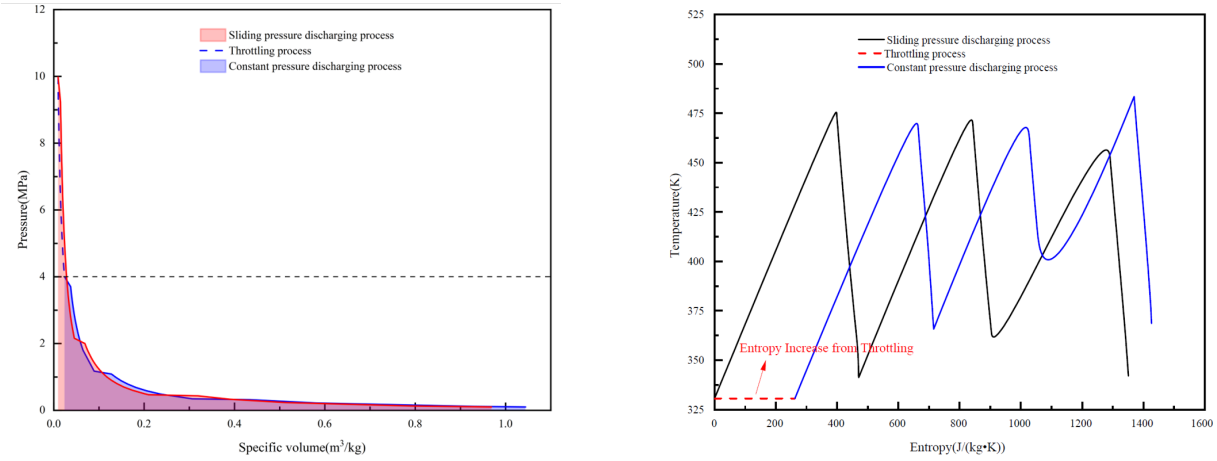

Figure 8. Thermodynamic comparison of energy release processes under different operating strategies: (a) P-v indicator diagram; (b) T-s temperature-entropy diagram

4.3.2 Dynamic response of key parameters

Figure 9 illustrates the dynamic evolution of key parameters during the energy storage and release phases. During the charge stage (Figure 9a), the constant pressure mode maintains stable gas storage pressure with initial compressor power consumption as high as 67.0 MW and minimal fluctuations. In the sliding pressure mode, gas storage pressure gradually increases, with initial compressor power consumption only 51.2 MW and load growing progressively. Although compressor efficiency fluctuates under sliding pressure conditions, the power savings from the reduced average pressure ratio significantly outweigh efficiency losses, resulting in a clear overall energy storage efficiency advantage. In the discharge stage (Figure 9b), the constant pressure mode maintains a steady output of approximately 65.6 MW by throttling the expander inlet pressure to 3.7 MPa via a regulating valve. However, the "pressure differential zone" between the wellhead and the expander inlet entails substantial throttling losses. In sliding pressure mode, the expander inlet pressure slides from 9.24 MPa to 3.70 MPa as wellhead pressure decreases, while output power gradually drops from 79.4 MW to 66.8 MW, yielding higher total electricity generation. During the initial energy release phase, the sliding pressure mode achieves a peak power output approximately 21% higher than the fixed pressure mode, indicating its superior ability to fully harness the energy potential during the high-pressure initial phase.

In summary, the sliding pressure mode outperforms the fixed pressure mode in both energy efficiency and economic viability by avoiding throttling losses, utilizing geothermal gains, and adapting to dynamic loads.

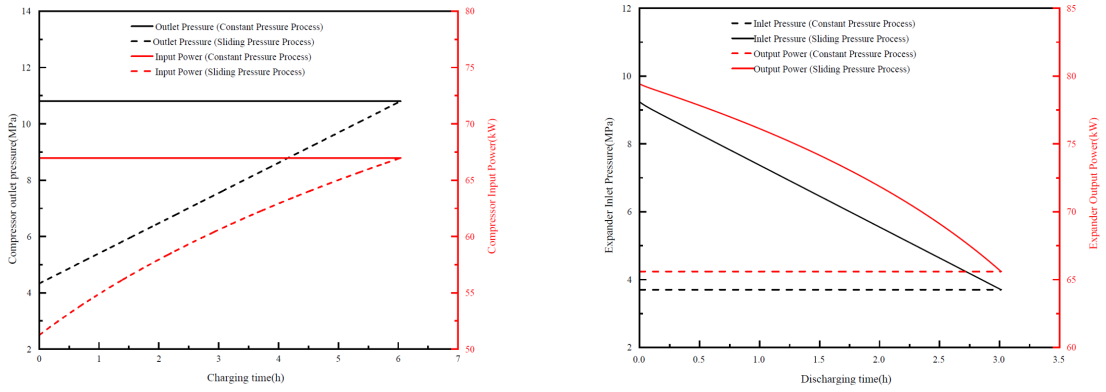

Figure 9. Dynamic response curves of key parameters during charge and discharge stages: (a) Compressor outlet pressure and power consumption; (b) Expander inlet pressure and output power

4.3.3 Full-cycle efficiency and exergy analysis

To quantify the fundamental differences between the two operating strategies, the full-cycle power loss distribution was calculated based on the Gouy–Stodola theorem (Table 3, Figure 10). Throttling power loss is the primary cause of low energy efficiency in constant-pressure mode, with the regulating valve accumulating irreversible external losses of 1.666×10^8 J. In contrast, the sliding-pressure mode completely eliminates this loss. Regarding internal energy losses: Expander energy losses in the sliding-pressure mode are slightly higher than in the fixed-pressure mode. Compressor energy losses decrease from 1.216×10^8 J in fixed-pressure mode to 1.139×10^8 J due to the reduced average pressure ratio. Overall, the incremental energy loss from variable operating conditions is far outweighed by the energy savings achieved by eliminating throttling.

Table 3. Comparison of system performance metrics across the entire lifecycle under different operational strategies

Performance Metrics	Electricity Consumption (kWh)	Electricity Generation (kWh)	Average Output Power (KW)	Energy Storage Density (ESD) ($kWh \cdot m^{-3}$)	System Round-Trip Efficiency (RTE) (%)	Total Throttling Loss (MJ)	Throttling Loss Rate (%)
Constant pressure	404.82	197.62	65.59	6.51	48.82	166.60	11.43
Sliding pressure	363.57	221.76	73.60	7.31	60.99	0	0

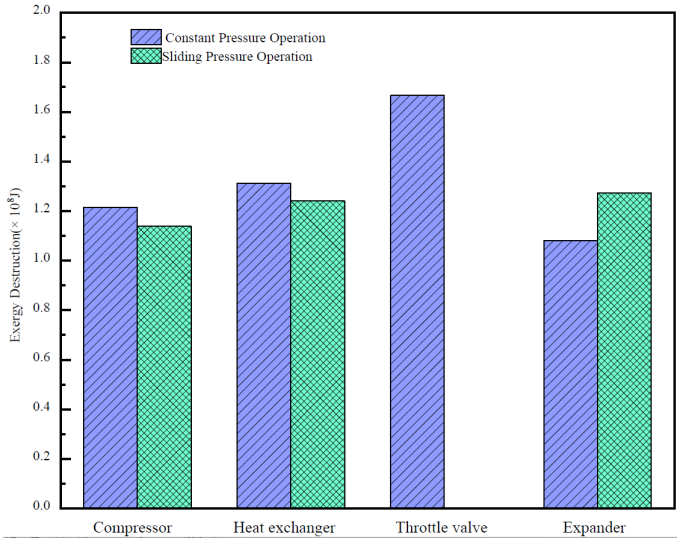

Figure 10. Comparison of cumulative exergy destruction distribution among key components over the full cycle

Leveraging these thermodynamic advantages, the sliding pressure strategy significantly outperforms the constant pressure mode in system RTE. By fully recovering pressure potential energy and synergistically utilizing deep well geothermal compensation, it achieves dual enhancements in work capacity and energy efficiency. Although constant-pressure mode delivers more stable power output, it incurs substantial thermodynamic costs. For abandoned-well AA-CAES systems prioritizing economic benefits, the sliding-pressure strategy better aligns with the large pressure differential and non-steady-state characteristics of deep-well storage chambers, making it the superior engineering choice.

This study demonstrates that sliding-pressure operation increases system efficiency by approximately 12.17%, significantly exceeding the 1.3% improvement reported in the study [36]. This discrepancy primarily stems from prior studies relying on adiabatic or weak heat exchange assumptions, which overlooked the "geothermal feedback" benefits triggered during sliding pressure operations. By integrating a coupled wellbore transient heat transfer model, this research captured approximately 576.69 MJ of geothermal gains, thereby more comprehensively revealing the true potential of sliding pressure strategies.

4.4 Sensitivity Analysis of Key Parameters

To provide a basis for engineering design, this section employs the variable disturbance method with the "constant wall temperature-sliding pressure" optimal operating condition as the reference to quantitatively identify the primary controlling factors affecting system performance.

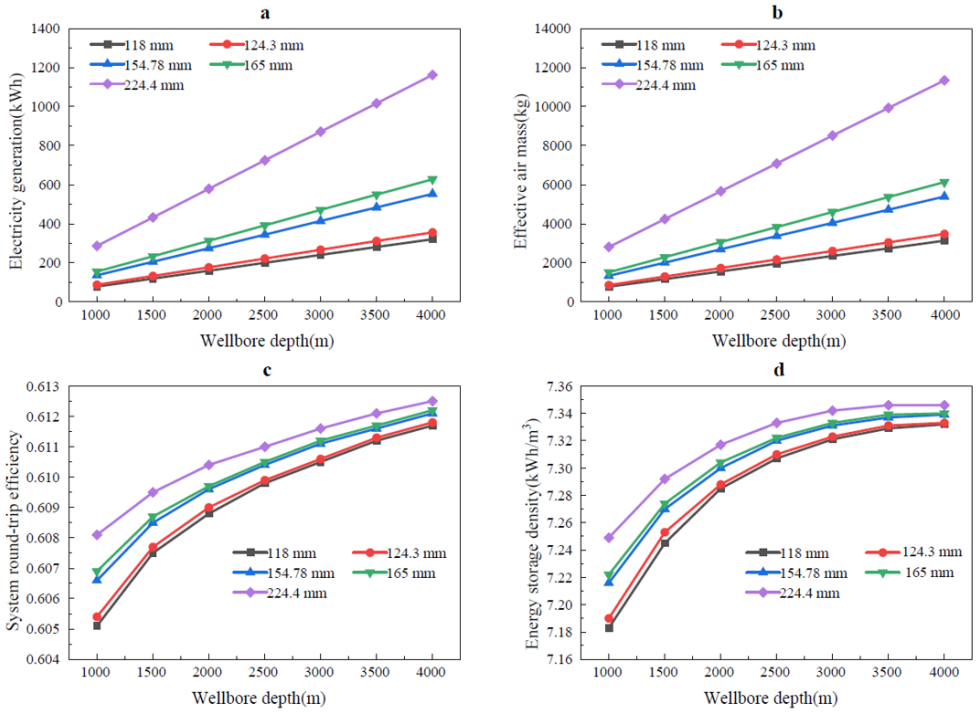

Figure 11. The impact of different wellbore depths and inner diameters on system performance

4.4.1 Wellbore geometric parameters

Wellbore depth and inner diameter jointly determine the system's thermodynamic boundary by coupling gas column potential energy, geothermal gradient, and flow resistance characteristics. Figure 11 reveals the nonlinear influence patterns of both factors on system performance.

Well depth is the primary factor governing energy throughput scale. Benefiting from the "geothermal-gravity combined pressurization" effect of deep gas columns, when well depth increases from 1000 m to 4000 m (at a reference inner diameter of 124.3 mm), effective gas storage capacity and single-cycle power generation surge by 308%. ESD exhibits significant depth dependency, steadily increasing from 7.19 kWh/m^3 to 7.33 kWh/m^3 with increasing well depth. Moreover, the evolution curves of ESD across different inner diameters highly overlap, confirming that the energy storage limit per unit volume is primarily controlled by depth—simply increasing the pipe diameter cannot overcome this physical upper bound. RTE reflects the competing mechanisms of flow resistance and heat transfer efficiency. Vertically, "thermal compensation" in deep formation rock causes RTE to increase monotonically with well depth. Horizontally, the influence of inner diameter exhibits pronounced diminishing marginal returns. Small diameters limit RTE due to high frictional losses; when diameter expands to 165 mm,

flow resistance effects are largely eliminated, and RTE approaches saturation. Notably, further increasing the inner diameter yields negligible efficiency gains due to diminished gas-wall heat exchange caused by reduced specific heat transfer area.

In summary, abandoned well rehabilitation should adhere to the principle of "prioritizing deep wells with moderate borehole diameters". It is recommended to select wells deeper than 2500 m with inner diameters exceeding 124 mm to achieve dual optimization of capacity gains and fluid transport efficiency.

4.4.2 Wellbore operating pressure

Operating pressure is the key parameter determining the system's energy density and the work done during compression/expansion. When the minimum pressure remains constant, increasing the maximum gas storage pressure P_{max} significantly enhances the system's ESD (Figure 12). When P_{max} increases from 8.0 MPa to 15.0 MPa, the effective gas storage mass rises from 1443.2 kg to 3984.5 kg. The ESD consequently jumps from 4.61 kWh/m^3 to 14.80 kWh/m^3, an increase exceeding 220%, indicating that pressure elevation is a direct and effective approach to enhancing the utilization rate of abandoned wells. The RTE increases with rising pressure but at a decelerating rate, exhibiting diminishing marginal returns: the RTE rose from 60.21% at 8 MPa to 62.22% at 15 MPa. Although increased pressure enhances enthalpy reduction, it also raises compressor outlet temperature, intensifying heat dissipation during energy storage. Balancing equipment pressure tolerance with efficiency gains, the 12–14 MPa range represents an optimal design window, achieving a favorable equilibrium between high energy density and superior cycle efficiency.

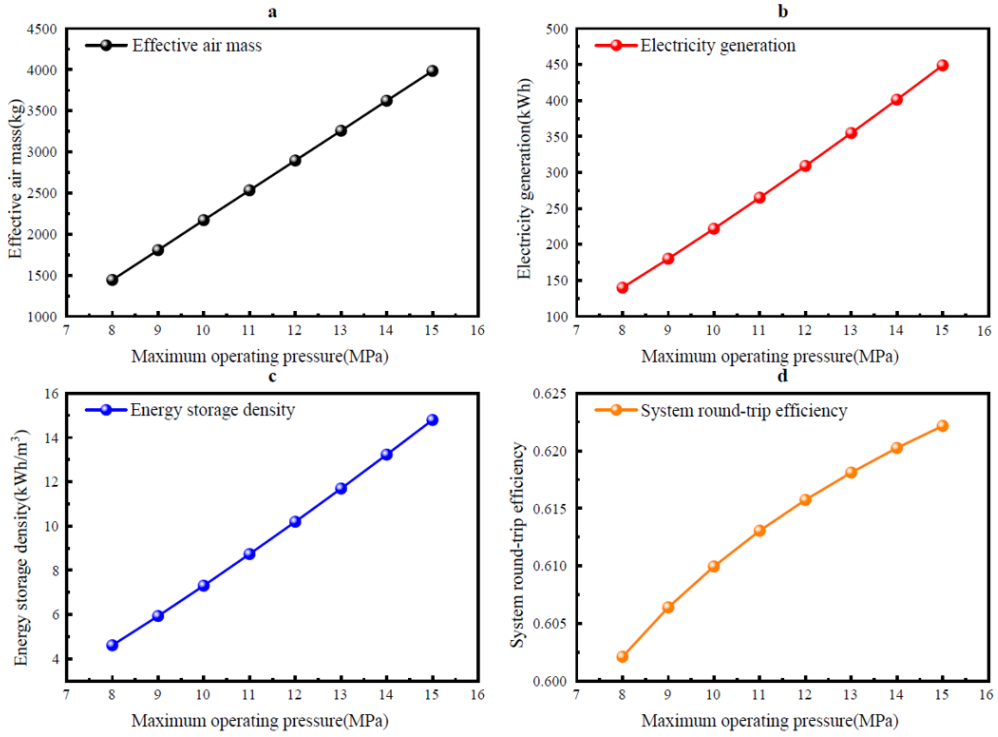

Figure 12. The impact of different wellbore operating pressure on system performance

4.4.3 Mass flow rate

Mass flow rate determines the adequacy of heat exchange by influencing the residence time of the working fluid within the wellbore. As shown in Figure 13, ESD exhibits a significant negative correlation with flow rate: when the gas injection rate is 0.05 kg/s, ESD peaks at 7.336 kWh/m^3; when the flow rate increases to 0.35 kg/s, ESD decreases to 7.184 kWh/m^3. The mechanism is that low flow rates prolong gas residence time, allowing sufficient release of compression heat to the surrounding rock. This lowers the wellbore temperature, increasing gas density under fixed upper pressure limits and producing a "thermally induced expansion" effect. Conversely, high flow rates cause heat accumulation, limiting effective gas charging. RTE similarly exhibits a "timescale effect": under low-flow conditions, heat exchange is thorough, geothermal compensation is saturated, and RTE peaks at 61.12%. As flow increases, heat transfer lag intensifies and geothermal contribution declines, reducing RTE to 60.39% at high flow rates.

In summary, "low flow rate" is key to leveraging the geothermal advantage of abandoned wells. This indicates that deep well AA-CAES systems are better suited for "long-duration energy storage" scenarios. Adopting low-flow, long-duration operation strategies can enhance efficiency while increasing storage capacity, achieving optimal techno-economic performance.

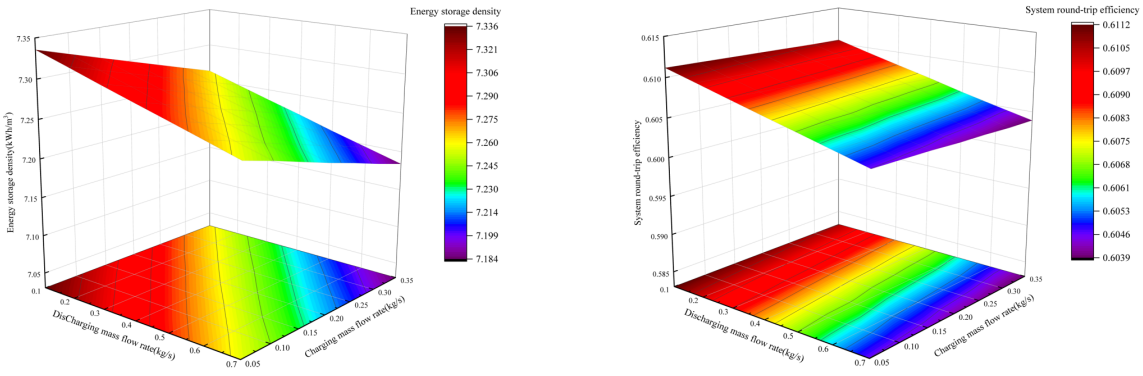

(a) (b)

Figure 13. Cloud map of the impact of different injection and production flow rates on system performance: (a) Energy storage density (ESD); (b) System round-trip efficiency (RTE)

4.4.4 Heat transfer characteristics

The coupling between ground heat exchanger efficiency and downhole convective heat transfer systems determines the thermal boundary conditions of the system, thereby exerting significant nonlinear effects on RTE and ESD (Figure 14). Simulation results indicate that system performance exhibits notable sensitivity to ground heat exchange efficiency. Under the reference operating condition (h_w = 15 W/m^2·K), increasing ε from 0.7 to 0.9 raises RTE from 50.83% to 60.99% and boosts ESD from 6.713 kWh/m^3 to 7.309 kWh/m^3. The mechanism lies in: high-efficiency heat recovery enhances the quality of expansion work, while high-efficiency cooling induces a "thermally induced volume expansion" effect, thereby effectively increasing ESD. In contrast, heat exchange on the wellbore side exhibits a pronounced "diminishing marginal returns" characteristic. Under ε = 0.9 conditions, even when h_w increases from 5 to 40 W/(m^2·K), RTE rises by only 0.64% and ESD by less than 1.8%. This phenomenon indicates a "rock thermal conductivity bottleneck" in abandoned well thermal storage, where the primary control mechanism shifts to internal rock thermal conduction. Overall, engineering designs should prioritize high-efficiency Printed Circuit Heat Exchanger ($\varepsilon \geq 0.85$) while maintaining appropriate wellbore roughness or introducing turbulence at low flow rates. This approach keeps h_w within 15–20 W/(m^2·K), achieving an optimal balance between technical feasibility and economic viability.

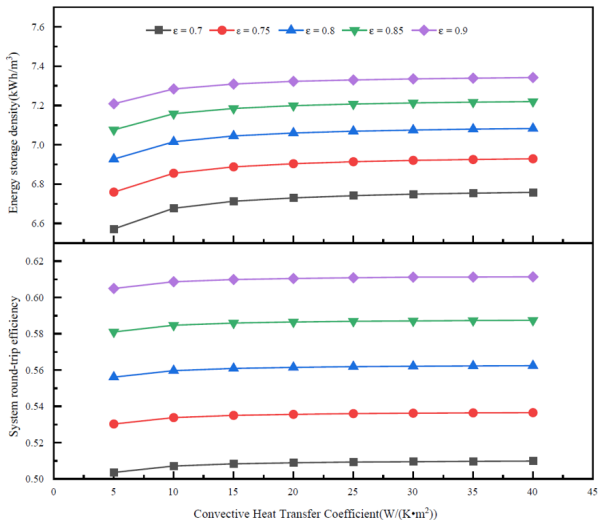

Figure 14. The Impact of different heat exchanger efficiency and convective heat transfer coefficient on system performance

4.4.5 Sensitivity ranking and controlling factors

Normalized sensitivity analysis of parameters indicates that the primary factors influencing system ESD are, in descending order: wellbore operating pressure > wellbore depth > injection/production flow rate > heat exchanger efficiency > wellbore bore diameter. Among these, the contribution of maximum pressure increase to storage capacity exhibits linear dominance. Factors affecting system RTE are ranked as: heat exchanger efficiency > operating strategy > injection/production flow rate > wellbore depth > wellbore bore diameter. These findings indicate that enhancing system energy efficiency requires prioritizing optimization of the surface heat exchange system and adopting a sliding pressure operating strategy; increasing energy storage capacity necessitates selecting deep, high-pressure-capacity abandoned wells. These conclusions apply to the design and optimization of AA-CAES systems utilizing abandoned oil and gas wells as storage cavities.

5 Conclusions

This paper establishes a comprehensive thermodynamic model for AA-CAES systems in abandoned oil and gas wells, coupling gas column gravity, geothermal gradient, and unsteady-state heat transfer in surrounding rock. It systematically evaluates the coupled effects of deep-well heat transfer mechanisms and operational strategies. Key conclusions are as follows:

(1) Revealed the unique "quasi-isothermal" heat storage characteristics of abandoned wells at low flow rates. The constant-wall-temperature model accurately captures rock mass heat exchange, correcting the 6.12% capacity prediction deviation of the adiabatic model, making it the optimal heat transfer model for deep well energy storage.

(2) Established the thermodynamic advantages of deep well sliding pressure operation. By eliminating throttling losses and activating the rock formation's "thermal compensation" effect, the sliding pressure strategy increased the system's RTE from 48.82% under constant pressure operation to 60.99%, recovering an additional 576.69 MJ of geothermal energy, demonstrating significant thermodynamic benefits.

(3) The mechanism of "thermally induced capacity enhancement" at low flow rates was elucidated. Low flow rates prolong thermal relaxation time, increasing ESD by 2.2% through this mechanism, confirming the system's suitability for "deep, long-duration, capacity-type" grid peak shaving applications.

(4) Key performance determinants and hierarchical optimization criteria were clarified. Sensitivity analysis indicates that operating pressure and well depth primarily govern ESD, while heat exchanger efficiency and operational strategies core-influence RTE. Engineering design should adhere to the principle of "prioritizing deep-well high-pressure sites and designing for sliding-pressure reheat matching".

This study, based on ideal gas and homogeneous rock assumptions, struggles to accurately simulate complex deep-well conditions and remains limited to single-well analysis. To advance large-scale engineering applications, future research will focus on: (1) Incorporating one-dimensional/two-dimensional distributed parameter models with real gas equations of state and heterogeneous geological models to enhance prediction accuracy under extreme high-pressure conditions; (2) Developing modularized series-parallel network scheduling models for tens to hundreds of wells to overcome single-well power limitations and smooth output fluctuations; (3) Exploring dynamic coupling mechanisms with wind and solar power plants to evaluate commercial potential within new power systems.

Author Contributions

Conceptualization, D.J.X. and Z.W.X.; methodology, Z.W.X.; software, Z.W.X.; validation, Z.W.X. and S.Q.N.; formal analysis, Z.W.X. and F.P.H.; investigation, Z.W.X.; resources, D.J.X.; data curation, Z.W.X.; writing—original draft preparation, Z.W.X.; writing—review and editing, D.J.X., Z.W.X., S.Q.N., and F.P.H.; visualization, Z.W.X.; supervision, D.J.X.; project administration, D.J.X. All authors have read and agreed to the published version of the manuscript.

Data Availability

The data used to support the findings of this study are available from the corresponding author upon request.

Conflicts of Interest

The authors declare no conflict of interest.

References

[1] A. M. I. Qureshy and I. Dincer, "A new integrated renewable energy system for clean electricity and hydrogen fuel production," *Int. J. Hydrogen Energy*, vol. 45, no. 41, pp. 20 944–20 955, 2020. https://doi.org/10.1016/j.ijhydene.2020.04.218

[2] M. J. B. Kabeyi and O. A. Olanrewaju, "Sustainable energy transition for renewable and low carbon grid electricity generation and supply," *Front. Energy Res.*, vol. 9, p. 743114, 2022. https://doi.org/10.3389/fenrg.2021.743114

[3] M. Mahmoud, M. Ramadan, A. G. Olabi, K. Pullen, and S. Naher, "A review of mechanical energy storage systems combined with wind and solar applications," *Energy Convers. Manage.*, vol. 210, p. 112670, 2020. https://doi.org/10.1016/j.enconman.2020.112670

[4] K. Hooman, "Heat commodification for a sustainable energy future," *Power Eng. Eng. Thermophys.*, vol. 3, no. 3, pp. 189–194, 2024. https://doi.org/10.56578/peet030304

[5] X. Bu, S. Huang, S. Liu, Y. Yang, J. Shu, X. Tang, H. Chen, and G. Wang, "Efficient utilization of abandoned mines for isobaric compressed air energy storage," *Energy*, vol. 311, p. 133392, 2024. https://doi.org/10.1016/j.energy.2024.133392

[6] A. B. Gallo, J. R. Simões-Moreira, H. K. M. Costa, M. M. Santos, and E. M. dos Santos, "Energy storage in the energy transition context: A technology review," *Renew. Sustain. Energy Rev.*, vol. 65, pp. 800–822, 2016. https://doi.org/10.1016/j.rser.2016.07.028

[7] M. Doering, "Assessment of storage options for reduction of yield losses in a region with 100% renewable electricity," *Energy Procedia*, vol. 73, pp. 218–230, 2015. https://doi.org/10.1016/j.egypro.2015.07.675

[8] K. Rouindej, E. Samadani, and R. A. Fraser, "A comprehensive data-driven study of electrical power grid and its implications for the design, performance, and operational requirements of adiabatic compressed air energy storage systems," *Appl. Energy*, vol. 257, p. 113990, 2020. https://doi.org/10.1016/j.apenergy.2019.113990

[9] K. Yang, Y. Zhang, X. Li, and J. Xu, "Theoretical evaluation on the impact of heat exchanger in advanced adiabatic compressed air energy storage system," *Energy Convers. Manage.*, vol. 86, pp. 1031–1044, 2014. https://doi.org/10.1016/j.enconman.2014.06.062

[10] Z. Han, Q. Hu, and P. Li, "Research on characteristics of CCHP system based on compressed air energy storage," *Acta Energiae Solaris Sinica*, vol. 43, no. 10, pp. 409–415, 2022. https://doi.org/10.19912/j.0254-0096.tynxb.2021-0406

[11] Y. Pang and Z. Han, "Off-design performance analysis of AA-CAES based on variable efficiency compressor," *Electric Power Construction*, vol. 37, no. 8, pp. 38–44, 2016. https://doi.org/10.3969/j.issn.1000-7229.2016.08.006

[12] P. Li, Q. Hu, and Z. Han, "Research on characteristics of AA-CAES system under different working mediums and heating storage mediums," *J. Chin. Soc. Power Eng.*, vol. 42, no. 4, pp. 372–379, 2022. https://doi.org/10.19805/j.cnki.jcspe.2022.04.011

[13] A. Mohammadi and M. Mehrpooya, "Exergy analysis and optimization of an integrated micro gas turbine, compressed air energy storage and solar dish collector process," *J. Clean. Prod.*, vol. 139, pp. 372–383, 2016. https://doi.org/10.1016/j.jclepro.2016.08.057

[14] J. C. Kurnia, M. S. Shatri, Z. A. Putra, J. Zaini, W. Caesarendra, and A. P. Sasmito, "Geothermal energy extraction using abandoned oil and gas wells: Techo-economic and policy review," *Int. J. Energy Res.*, vol. 46, no. 1, pp. 28–60, 2022. https://doi.org/10.1002/er.6386

[15] J. Ezekiel, A. Ebigbo, B. M. Adams, and M. O. Saar, "Combining natural gas recovery and CO_2-based geothermal energy extraction for electric power generation," *Appl. Energy*, vol. 269, p. 115012, 2020. https://doi.org/10.1016/j.apenergy.2020.115012

[16] J. Huang, X. Ge, H. Ma, T. Zhao, Y. Li, and X. Shi, "A study on thermodynamic coupling in dynamic injection and production processes of compressed air energy storage," *Energy*, vol. 319, p. 135093, 2025. https://doi.org/10.1016/j.energy.2025.135093

[17] F. Schmidt, J. Menéndez, H. Konietzky, Z. Jiang, J. M. Fernández-Oro, L. Álvarez, and A. Bernardo-Sánchez, "Technical feasibility of lined mining tunnels in closed coal mines as underground reservoirs of compressed air energy storage systems," *J. Energy Storage*, vol. 78, p. 110055, 2024. https://doi.org/10.1016/j.est.2023.110055

[18] L. Ma, X. Zhang, T. Zhang, X. Xue, X. Chen, and Y. Si, "Design and operation of an adiabatic compressed air energy storage system incorporating a detailed heat exchanger model," *Energy*, vol. 304, p. 132104, 2024. https://doi.org/10.1016/j.energy.2024.132104

[19] S. Sarmast, R. A. Fraser, and M. B. Dusseault, "Performance and cyclic heat behavior of a partially adiabatic cased-wellbore compressed air energy storage system," *J. Energy Storage*, vol. 44, p. 103279, 2021. https://doi.org/10.1016/j.est.2021.103279

[20] S. Houssainy, M. Janbozorgi, P. Ip, and P. Kavehpour, "Thermodynamic analysis of a high temperature hybrid compressed air energy storage (HTH-CAES) system," *Renew. Energy*, vol. 115, pp. 1043–1054, 2018. https://doi.org/10.1016/j.renene.2017.09.038

[21] Q. Zhang, A. Dahi Taleghani, and D. Elsworth, "Underground energy storage using abandoned oil & gas wells assisted by geothermal," *J. Energy Storage*, vol. 110, p. 115317, 2025. https://doi.org/10.1016/j.est.2025.115317

[22] Z. Han, S. Liu, Q. Zhou, and Y. Peng, "Performance analysis of AA-CAES system with constant wall-temperature air storage model," *Proc. CSEE*, vol. 36, no. 12, pp. 3373–3381, 2016. https://doi.org/10.13334/j.0258-8013.pcsee.150454

[23] S. Mucci, A. Bischi, S. Briola, and A. Baccioli, "Small-scale adiabatic compressed air energy storage: Control strategy analysis via dynamic modelling," *Energy Convers. Manage.*, vol. 243, p. 114358, 2021. https://doi.org/10.1016/j.enconman.2021.114358

[24] G. Manfrida and R. Secchi, "Performance prediction of a small-size adiabatic compressed air energy storage system," *Int. J. Thermodyn.*, vol. 18, no. 2, pp. 111–119, 2015. https://doi.org/10.5541/ijot.5000071710

[25] V. Tola, V. Meloni, F. Spadaccini, and G. Cau, "Performance assessment of adiabatic compressed air energy storage (A-CAES) power plants integrated with packed-bed thermocline storage systems," *Energy Convers. Manage.*, vol. 151, pp. 343–356, 2017. https://doi.org/10.1016/j.enconman.2017.08.051

[26] A. M. Al Jubori and Q. A. Jawad, "Investigation on performance improvement of small scale compressed-air energy storage system based on efficient radial-inflow expander configuration," *Energy Convers. Manage.*, vol. 182, pp. 224–239, 2019. https://doi.org/10.1016/j.enconman.2018.12.048

[27] C. Diyoke and U. Ngwaka, "Numerical comparison of two operating modes of thermal energy storage tank for compression heat storage in adiabatic compressed air energy storage," *J. Energy Storage*, vol. 30, p. 101558, 2020. https://doi.org/10.1016/j.est.2020.101558

[28] Z. Han, S. Wang, Z. Hu, L. Zhu, and L. Guo, "Study on operation strategy of AA-CAES+CSP system," *Acta Energiae Solaris Sinica*, vol. 42, no. 1, pp. 423–430, 2021. https://doi.org/10.19912/j.0254-0096.tynxb.2018-0630

[29] Y. Cui, T. Jiang, and Z. Chen, "A constant-pressure air storage operation strategy for an isothermal compressed air energy storage system based on a linear-drive liquid piston," *Energies*, vol. 18, no. 12, p. 3178, 2025. https://doi.org/10.3390/en18123178

[30] F. Xiao, W. Chen, B. Zhang, T. Zhang, N. Xie, Z. Wang, H. Chen, and X. Xue, "A novel constant power operation mode of constant volume expansion process for AA-CAES: Regulation strategy, dynamic simulation, and comparison," *Energy*, vol. 284, p. 128594, 2023. https://doi.org/10.1016/j.energy.2023.128594

[31] S. Sarmast, K. Rouindej, R. A. Fraser, and M. B. Dusseault, "Optimizing near-adiabatic compressed air energy storage (NA-CAES) systems: Sizing and design considerations," *Appl. Energy*, vol. 357, p. 122465, 2024. https://doi.org/10.1016/j.apenergy.2023.122465

[32] Y. Zhang, Y. Wu, and K. Yang, "Dynamic characteristics of a two-stage compression and two-stage expansion compressed carbon dioxide energy storage system under sliding pressure operation," *Energy Convers. Manage.*, vol. 254, p. 115218, 2022. https://doi.org/10.1016/j.enconman.2022.115218

[33] D. Pottie, B. Cardenas, S. Garvey, J. Rouse, E. Hough, A. Bagdanavicius, and E. Barbour, "Comparative analysis of isochoric and isobaric adiabatic compressed air energy storage," *Energies*, vol. 16, no. 6, p. 2646, 2023. https://doi.org/10.3390/en16062646

[34] A. R. Razmi, M. Soltani, C. Aghanajafi, and M. Torabi, "Thermodynamic and economic investigation of a novel integration of the absorption-recompression refrigeration system with compressed air energy storage (CAES)," *Energy Convers. Manage.*, vol. 187, pp. 262–273, 2019. https://doi.org/10.1016/j.enconman.2019.03.010

[35] N. M. Jubeh and Y. S. H. Najjar, "Green solution for power generation by adoption of adiabatic CAES system," *Appl. Therm. Eng.*, vol. 44, pp. 85–89, 2012. https://doi.org/10.1016/j.applthermaleng.2012.04.005

[36] Z. Han, Y. Sun, P. Li, and Q. Hu, "Comparative study on performance of two AA-CAES systems under different output modes," *Acta Energiae Solaris Sinica*, vol. 43, no. 5, pp. 60–66, 2022. https://doi.org/10.19912/j.0254-0096.tynxb.2020-0474

[37] H. Mozayeni, M. Negnevitsky, X. Wang, F. Cao, and X. Peng, "Performance study of an advanced adiabatic compressed air energy storage system," *Energy Procedia*, vol. 110, pp. 71–76, 2017. https://doi.org/10.1016/j.egypro.2017.03.108

[38] C. S. Brown and G. Falcone, "Investigating heat transmission in a wellbore for low-temperature, open-loop geothermal systems," *Therm. Sci. Eng. Prog.*, vol. 48, p. 102352, 2024. https://doi.org/10.1016/j.tsep.2023.102352